Simple and Robust Differentiation of Human Pluripotent Stem Cells toward Chondrocytes by Two Small-Molecule Compounds

Manabu Kawata,[1,2] Daisuke Mori,[1,2] Kosuke Kanke,[3] Hironori Hojo,[3] Shinsuke Ohba,[3] Ung-il Chung,[3] Fumiko Yano,[2,3] Hideki Masaki,[4] Makoto Otsu,[4] Hiromitsu Nakauchi,[4,5] Sakae Tanaka,[1] and Taku Saito[1,2,*]

[1]Sensory & Motor System Medicine, Faculty of Medicine, The University of Tokyo, Tokyo, Japan
[2]Bone and Cartilage Regenerative Medicine, Faculty of Medicine, The University of Tokyo, Tokyo, Japan
[3]Center for Disease Biology and Integrative Medicine, Faculty of Medicine, The University of Tokyo, Tokyo, Japan
[4]Division of Stem Cell Therapy, Center for Stem Cell Biology and Regenerative Medicine, Institute of Medical Science, The University of Tokyo, Tokyo, Japan
[5]Institute for Stem Cell Biology and Regenerative Medicine, Stanford University School of Medicine, Stanford, CA, USA
*Correspondence: tasaitou-tky@umin.ac.jp
https://doi.org/10.1016/j.stemcr.2019.07.012

SUMMARY

A simple induction protocol to differentiate chondrocytes from pluripotent stem cells (PSCs) using small-molecule compounds is beneficial for cartilage regenerative medicine and mechanistic studies of chondrogenesis. Here, we demonstrate that chondrocytes are robustly induced from human PSCs by simple combination of two compounds, CHIR99021, a glycogen synthase kinase 3 inhibitor, and TTNPB, a retinoic acid receptor (RAR) agonist, under serum- and feeder-free conditions within 5–9 days. An excellent differentiation efficiency and potential to form hyaline cartilaginous tissues *in vivo* were demonstrated. Comprehensive gene expression and open chromatin analyses at each protocol stage revealed step-by-step differentiation toward chondrocytes. Genome-wide analysis of RAR and β-catenin association with DNA showed that retinoic acid and Wnt/β-catenin signaling collaboratively regulated the key marker genes at each differentiation stage. This method provides a promising cell source for regenerative medicine and, as an *in vitro* model, may facilitate elucidation of the molecular mechanisms underlying chondrocyte differentiation.

INTRODUCTION

Chondrocytes play pivotal roles in skeletal development and lifelong maintenance of articular cartilage. Disruption of their latter function can lead to osteoarthritis (OA), one of the most prevalent musculoskeletal disorders. The transcription factor SOX9 is expressed in all chondroprogenitors during chondrogenesis (Zhao et al., 1997), and directly regulates expression of extracellular matrix molecules including type 2 and type 11 collagens (COL2A1 and COL11A2, respectively), and Aggrecan (ACAN) (Bridgewater et al., 1998; Lefebvre et al., 1997; Sekiya et al., 2000).

Pluripotent stem cells (PSCs), such as human embryonic stem cells (ESCs) and human induced pluripotent stem cells (hiPSCs), are a promising cell source for treating degenerative diseases such as OA because of their unlimited expansion potential. They are also valuable experimental tools for *in vitro* studies of cell differentiation, including chondrogenesis. Several efficient methods have been developed for chondrocyte induction from human PSCs, and they are based on the sequence of pathways active during chondrogenesis and employ many kinds of cytokines (Craft et al., 2015; Oldershaw et al., 2010; Yamashita et al., 2015). In addition to gene transduction or cytokine treatments, recent protocols for cell reprogramming or differentiation have used small-molecule compounds, which have definite advantages over previous methods. Small-molecule compounds are easy to use, can be efficiently delivered to cells, are non-immunogenic, and are more cost-effective (Araoka et al., 2014; Cao et al., 2016; Kanke et al., 2014). Their effects can be finely regulated by adjusting the concentrations and combinations (Cao et al., 2016). Therefore, development of a simple induction protocol to obtain chondrocytes from PSCs using small-molecule compounds will benefit cartilage regenerative medicine and mechanistic studies of chondrocyte differentiation.

Canonical Wnt signaling regulates mesendoderm induction of PSCs (Bakre et al., 2007). We previously employed CHIR99021, a compound that activates canonical Wnt signaling by suppressing β-catenin degradation through glycogen synthase kinase (GSK) 3β inhibition, in the initial step of osteoblast differentiation of mouse ESCs (mESCs) (Kanke et al., 2014). Because chondrocytes are also derived from mesendodermal cells (Craft et al., 2015; Oldershaw et al., 2010; Yamashita et al., 2015), treatment of PSCs with CHIR99021 will be useful in the initial step of chondrogenesis. Moreover, retinoic acid (RA) and retinoids have been widely used to differentiate PSCs into various types of cells (Araoka et al., 2014; D'Amour et al., 2006; Hu et al., 2009; Osakada et al., 2008; Tonge and Andrews, 2010). While RA and retinoids suppress collagen production or cartilage matrix synthesis in chondrocytes cultures (Pacifici, 2018), they play essential roles in the process of limb bud formation and subsequent chondrogenesis during skeletal development (Niederreither et al., 1999, 2002). Thus, RA and retinoids may be useful for inducing chondrocytes from PSCs.

Here, we found that the simple combination of two small-molecule compounds, a WNT activator and an RA receptor (RAR) agonist, robustly induced chondrocytes from hiPSCs under serum- and feeder-free conditions within 5–9 days. Its excellent efficiency and the potential of the differentiated cells to form hyaline cartilaginous tissues *in vivo* were demonstrated. We also analyzed time-course gene expression and open chromatin profiles at each stage, as well as RAR and β-catenin association with DNA in the differentiation process.

RESULTS

Combination of CHIR99021 and TTNPB Induces Chondrogenic Markers in hiPSCs

We first examined the effects of CHIR99021 on mesendoderm differentiation of hiPSCs. Mesendoderm markers *T* and *MIXL1* were highly upregulated after 2 or 3 days of treatment with CHIR99021 at concentrations greater than 5 μM (Figure 1A). Cell viability was markedly impaired by 20 μM CHIR99021. As an additional compound to induce the cells toward chondrocytes, we selected TTNPB (4-[(E)-2-(5,6,7,8-tetrahydro-5,5,8,8-tetramethyl-2-naphthalenyl)-1-propenyl]benzoic acid), a selective pan-RAR agonist. Cells were treated with various doses of TTNPB for 5 days, along with an initial 2-day treatment by 10 μM CHIR99021. At greater than 10 nM TTNPB, expression of chondrogenic markers *SOX9*, *SOX5*, *COL2A1*, and *COL11A2* was greatly induced (Figure 1B). To investigate the timing of TTNPB treatment, we began 100 nM TTNPB treatment on day 0, 1, 2, or 3, then cultured the cells until day 5 or day 9. Expression of the chondrogenic markers was maximal when TTNPB was started on day 0 (Figure 1C). We then investigated the optimal CHIR99021 dose in combination with 100 nM TTNPB. Although *T* and *MIXL1* were induced in a dose-dependent manner on day 2 (Figure 1D), the chondrogenic markers were significantly elevated only when more than 5 μM CHIR99021 was applied, and these markers were not upregulated by treatment with less than 3 μM CHIR99021 (Figure 1E). Finally, we examined the optimal time period for CHIR99021 treatment. All four chondrogenic markers were efficiently upregulated on day 5 when 10 μM CHIR99021 was applied for the initial 2 days, in combination with 5 days of treatment with 100 nM TTNPB (Figure 1F). Based on these results, the optimized protocol was combined treatment with 5–10 μM CHIR99021 for the initial 2 days, and greater than 10 nM TTNPB for the whole period. Within these conditions, we chose 10 μM CHIR99021 treatment for the initial 2 days and 100 nM TTNPB for the whole period as the standard two-compound (2C) protocol (Figure 1G). This protocol was used for all subsequent analyses.

The 2C Protocol Differentiates hiPSCs toward Chondrocytes via Mesendoderm and Mesoderm Stages

We next examined the time dependence of changes in marker gene expression during differentiation induced by the 2C protocol. Decreased expression of pluripotent markers *NANOG* and *OCT4*, and increased expression of *T* and *MIXL1*, occurred immediately after the initiation of 2C treatment (Figure 2A). Paraxial mesoderm markers *TBX6* and *MEOX1* were sequentially upregulated from day 2 to day 4. Among lateral plate mesoderm markers, expression of *HAND1* was also increased on day 4, while *NKX2.5*, an early cardiomyocyte marker, was not upregulated during the differentiation; these findings indicate that a mixture of both paraxial mesodermal cells and lateral plate mesodermal cells was produced by the 2C protocol. Expression of *SOX9*, *SOX5*, and *SOX6*, essential transcription factors for chondrogenesis, was then increased, accompanied by upregulation of cartilage matrix genes including *COL2A1*, *COL11A2*, and *ACAN* (Figure 2A). As for articular cartilage-related genes, the expression level of *GDF5* was significantly increased along with differentiation, whereas *PRG4* (encoding Lubricin, known as an articular superficial zone protein) was not upregulated at all. Finally, expression of hypertrophic chondrocyte markers *COL10A1*, *VEGFα*, and *IHH* did not show significant upregulation up to day 21 (Figure 2A). Based on these marker gene expression patterns, we characterized four differentiation stages, namely pluripotent (day 0), mesendoderm (days 1–2), mesoderm (days 2–4), and chondrocyte stages (beginning on day 5) (Figure 2B). After initiation of the 2C protocol, the hiPSC-derived cells immediately began to grow outside of their colonies and continued proliferating (Figure 2C). The cell number plateaued on days 4–5 (Figure 2D).

The 2C Protocol Has Excellent Differentiation Efficiency

To examine the efficiency and homogeneity of 2C-induced differentiation, we performed immunofluorescence cytochemistry and fluorescence-activated cell sorting (FACS) analysis. NANOG and OCT4 were highly expressed in undifferentiated cells, but were not detectable after 9 days of differentiation (Figure 3A). SOX9 and COL2 were detected in almost all differentiated cells on day 9 (Figure 3A). FACS confirmed the differentiation efficiency (Figures 3B and 3C). Notably, NANOG- or OCT4-positive cells were not detected after differentiation, while 97.0% of cells were positive for SOX9 (Figure 3C).

hiPSC-Derived Cells Form Hyaline Cartilaginous Tissues *In Vivo*

We next transplanted hiPSC-derived cells differentiated by the 2C protocol into subcutaneous spaces and articular
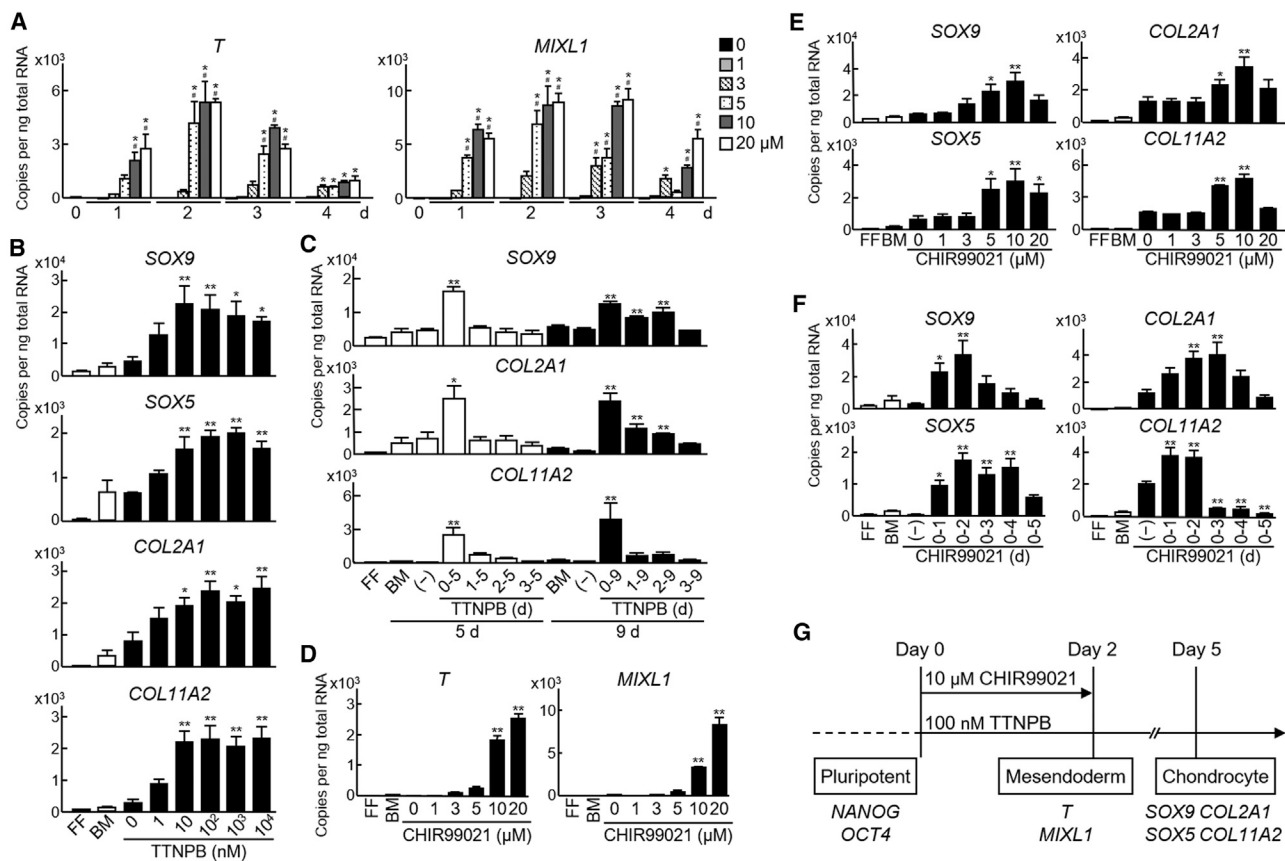
Figure 1. Optimization of Mesendoderm and Chondrocyte Differentiation of hiPSCs Using Two Compounds

(A) Optimization of dose and treatment period of CHIR99021 for mesendoderm differentiation. Cells were treated with various doses of CHIR99021 for up to 4 days. #p < 0.05 versus day 0; *p < 0.05 versus 0 μM in the same time period; Dunnett's test.

(B) Chondrocyte differentiation after 5 days of treatment with various TTNPB doses. Cells were also treated with 10 μM CHIR99021 for the initial 2 days. *p < 0.05, **p < 0.01 versus 0 nM; Dunnett's test.

(C) Optimization of timing to start 100 nM TTNPB treatment. Cells also received 10 μM CHIR99021 for the initial 2 days. *p < 0.05, **p < 0.01 versus (−); Dunnett's test.

(D and E) Mesendoderm differentiation after 2 days (D), or chondrocyte differentiation after 5 days (E) of treatment with various doses of CHIR99021. Cells also received 100 nM TTNPB throughout. *p < 0.05, **p < 0.01 versus 0 μM; Dunnett's test.

(F) Optimization of the treatment period of 10 μM CHIR99021 with 100 nM TTNPB treatment throughout. *p < 0.05, **p < 0.01 versus (−); Dunnett's test.

(G) Standard 2C protocol to induce chondrocytes from hiPSCs.

All mRNA levels are expressed as means ± SE (n = 9 replicates from three independent experiments). In (B) to (F): FF, hiPSCs under feeder-free conditions on day 0; BM, hiPSCs cultured in basal differentiation medium.

cartilage defects of mice to evaluate cartilage maturation *in vivo*. We seeded 1.7×10^6 differentiated cells into a small cylinder and cultured them for 1 week to form particles, as described previously (Saito et al., 2015). First, the particles were transplanted into subcutaneous spaces of NOD/SCID mice. After 8 weeks, hyaline cartilaginous tissues were observed in the transplantation sites by Safranin-O staining (Figure 3D). COL2-positive areas corresponded to the Safranin-O-positive areas, while COL10 immunofluorescence was not detectable (Figure 3E). Lubricin was expressed

in the surrounding layers just outside of the hyaline cartilaginous tissues (Figure 3E). Immunofluorescence with an anti-human vimentin antibody then showed that both the hyaline cartilaginous and the Lubricin-expressing tissues were derived from hiPSCs (Figure 3E). There were no signs of teratoma or other tumor formation around the transplantation sites or in other organs.

Next, the particles were transplanted into cartilage defects created in the trochlear grooves of femurs of NOD/SCID mice. After 6 months, Safranin-O staining confirmed
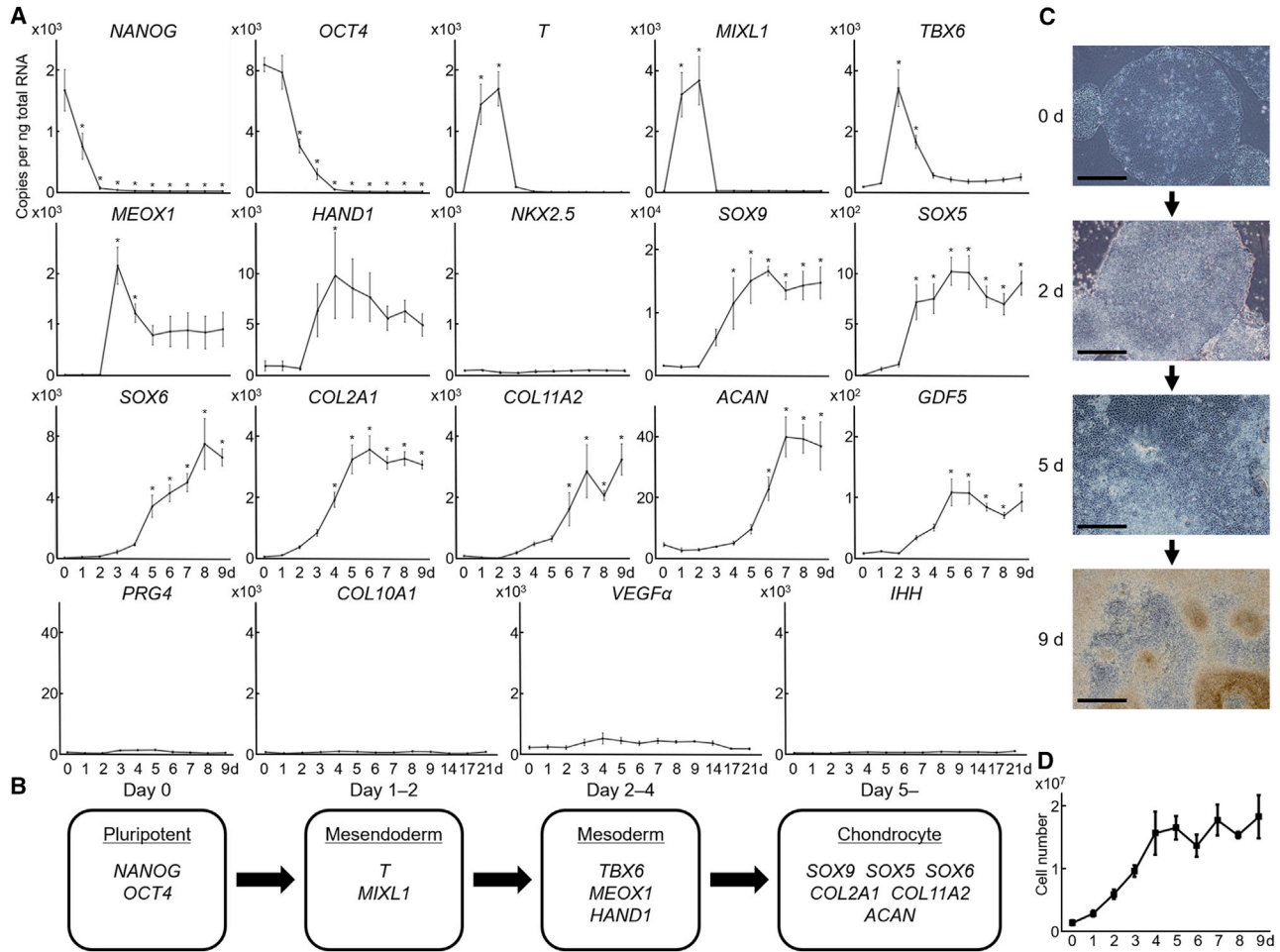
Figure 2. Time Course of Chondrocyte Differentiation from hiPSCs Using the 2C Protocol

(A) Time course of marker gene expression levels. Cells were treated with CHIR99021 for the initial 2 days and 100 nM TTNPB throughout. Data are expressed as means ± SE (n = 9 replicates from three independent experiments). *p < 0.05 versus day 0; Dunnett's test.

(B) Scheme showing step-by-step differentiation of hiPSCs by the 2C protocol.

(C) Morphology of hiPSC-derived differentiating cells at each stage of the 2C protocol. Scale bars, 500 μm.

(D) Cell proliferation during differentiation induced by the 2C protocol. Data are expressed as means ± SE (n = 9 replicates from three independent experiments).

See also Figure S1.

hyaline cartilaginous tissues in the transplanted defects, whereas almost no cartilage tissue formation or regeneration was observed in the defects without transplantation (Figure 3F). Histological scores of cellular morphology and Safranin-O staining of cartilage defects in the transplantation group were significantly higher than those in the non-transplantation group (Figure 3G). The regenerated tissues in the defects with transplantation exhibited strong COL2 expression comparable with the adjacent intact articular cartilage, whereas COL2 immunofluorescence was not detectable in the defects without transplantation (Figure 3H). Expression of COL10 was not observed in the transplantation sites, while Lubricin was expressed mainly

in surface layers of the regenerated tissues after transplantation (Figure 3H). Furthermore, immunofluorescence for human vimentin showed that tissues in the transplantation sites contained cells derived from hiPSCs (Figure 3H). No signs of teratoma or other tumor formation were seen around the transplanted joints or in other organs.

The 2C Protocol Induces Chondrocytes More Efficiently Than Protocols Using Cytokines

To further characterize differentiated cells produced by the 2C protocol, we compared their expression levels of marker genes with cells after differentiation by two other reported protocols using cytokines for about 2 weeks (Oldershaw
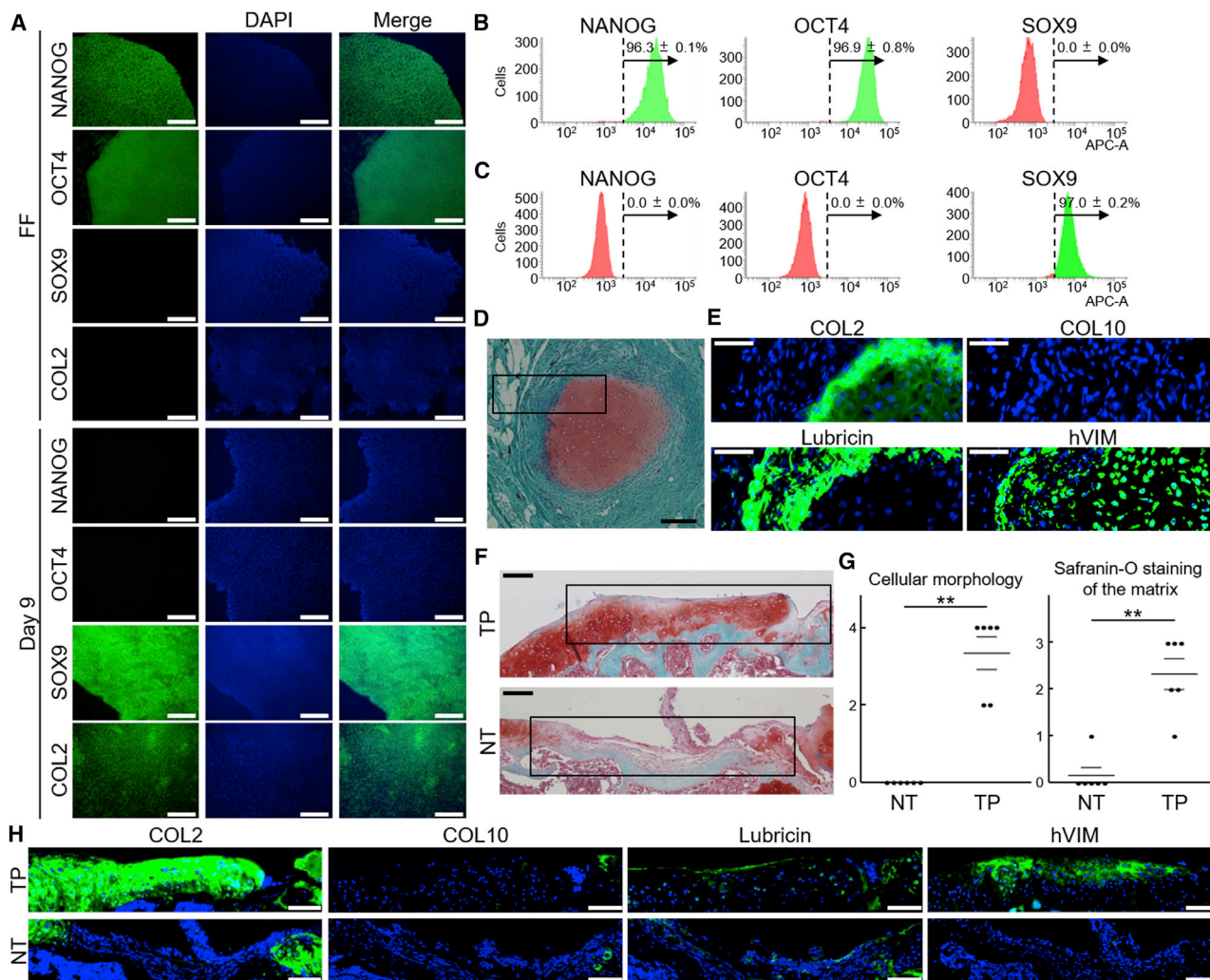
Figure 3. Evaluation of Differentiation Efficiency Using the 2C Protocol, and Transplantation of hiPSC-Derived Differentiated Cells into Subcutaneous Spaces and Articular Cartilage Defects in Mice

(A) Immunofluorescence cytochemistry of marker proteins in hiPSCs under feeder-free conditions (FF) on day 0 and in differentiated cells after 9 days of culture under the 2C protocol (day 9). Representative images from three independent experiments per condition are shown. Scale bars, 200 μm.

(B and C) FACS analysis of hiPSCs under feeder-free conditions (B) and differentiated cells after 9 days of culture under the 2C protocol (C) using antibodies against NANOG, OCT4, or SOX9. Representative plots of nine samples per condition are shown. Positive cell rates are shown as means ± SE (n = 9 replicates from three independent experiments).

(D) Safranin-O staining of subcutaneous transplantation sites after 8 weeks. Representative images of n = 6 mice are shown. A rectangle indicates the area enlarged in the immunofluorescence images in (E). Scale bars, 100 μm.

(E) Immunofluorescence of COL2, COL10, Lubricin, and human vimentin (hVIM) with DAPI labeling of nuclei in subcutaneous transplantation sites. Scale bars, 50 μm.

(F) Safranin-O staining of transplanted and non-transplanted defects created in articular cartilage of knees at 6 months after transplantation. Representative images of n = 6 mice per group are shown. Rectangles indicate the areas enlarged in the immunofluorescence images in (H). Scale bars, 200 μm.

(G) Histological scores of cartilage defects in transplantation and non-transplantation groups. Scores are expressed as means ± SE (n = 6 mice per group). **p < 0.01; Brunner-Munzel test.

(H) Immunofluorescence of COL2, COL10, Lubricin, and hVIM with DAPI labeling of nuclei in transplanted and non-transplanted cartilage defects. Scale bars, 100 μm.

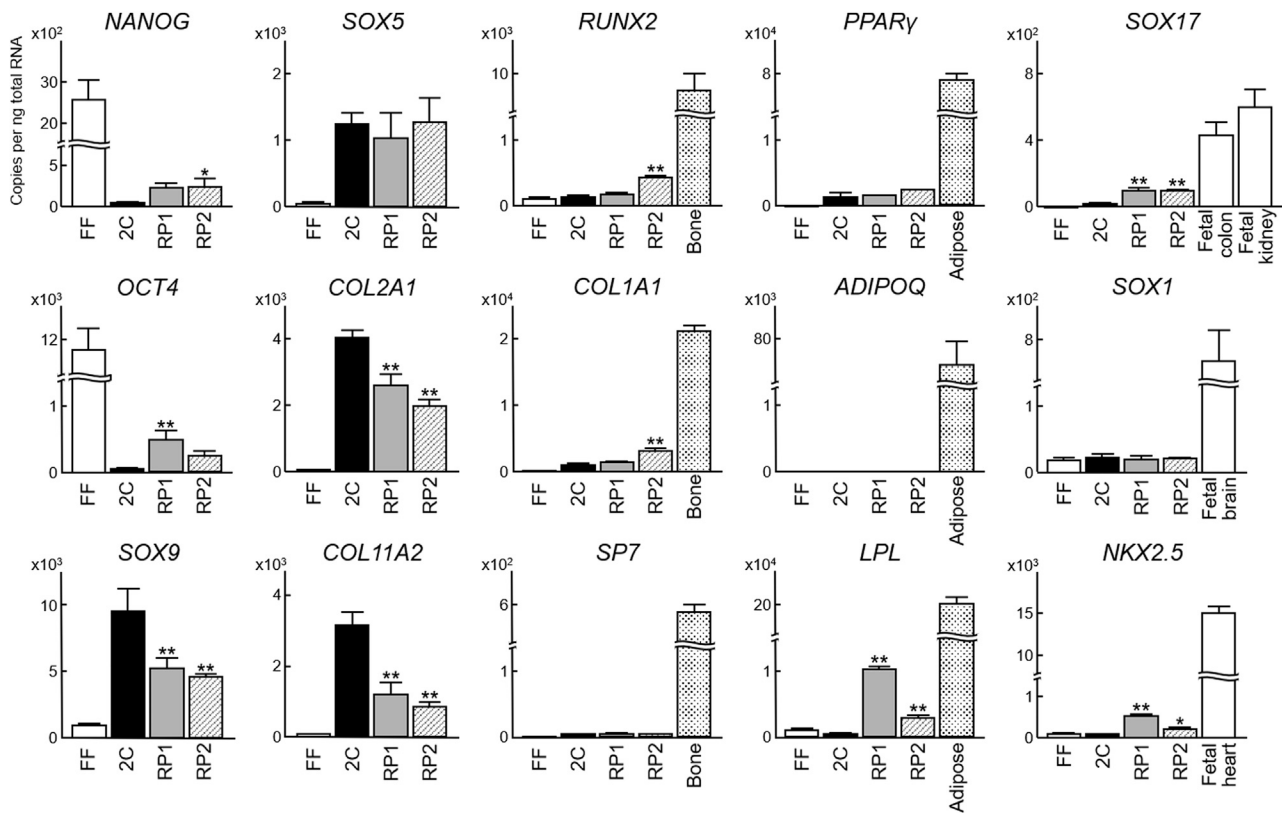In (F) to (H): TP, transplantation; NT, non-transplantation. See also Figure S1.

Figure 4. Marker Gene Expression in Cells Differentiated by the 2C Protocol or Representative Methods Using Cytokines
FF, hiPSCs under feeder-free conditions on day 0; 2C, cells after 9 days of differentiation induced by the 2C protocol; RP1, cells after 13 days of differentiation induced by a previously described method (Oldershaw et al., 2010); RP2, cells after 14 days of differentiation induced by another previously described method (Yamashita et al., 2015). Bone and Adipose, human bone and adipose tissue obtained from individuals undergoing knee arthroplasty. RNA of human fetal samples was obtained commercially. mRNA levels are expressed as means ± SE (n = 9 replicates from three independent experiments). *p < 0.05, **p < 0.01 versus 2C; Dunnett's test comparing 2C, RP1, and RP2.

et al., 2010; Yamashita et al., 2015). Expression levels of pluripotent and chondrogenic markers were significantly decreased and increased, respectively, by 2C differentiation compared with the other protocols (Figure 4). Expression of osteogenic markers, such as *RUNX2* and *COL1A1*, was significantly lower after 2C differentiation than after differentiation by one of the cytokine protocols, while the expression level of *SP7*, also an osteogenic marker, was similar among the protocols (Figure 4). Among adipogenic markers, expression of *PPARγ* and *ADIPOQ* was not different among the protocols, whereas the expression level of *LPL* was lower after 2C differentiation than differentiation by the cytokine protocols (Figure 4). Expression of an endoderm marker, *SOX17*, and an early cardiomyocyte marker, *NKX2.5*, was significantly suppressed after 2C differentiation, although expression of a neuroectoderm marker, *SOX1*, was not different among the protocols (Figure 4). Based on these data, we cannot conclude superiority for any method because the concepts and aims of the protocols were different. Nonetheless, our comparison showed that the

2C protocol induced chondrocytes from hiPSCs more efficiently when compared with these other protocols.

The 2C Protocol Induces Chondrocytes from Different hiPSC Clones and mESCs
To confirm reproducibility of 2C-induced differentiation, we subjected different hiPSC clones to the protocol. Expression levels of marker genes and differentiation efficiency were similar among the hiPSC clones (Figures S1A–S1F). We next performed differentiation by the 2C protocol using mESCs adapted to feeder-free conditions. Although expression of pluripotent marker genes was decreased more slowly in mESCs than in hiPSCs, the increase in chondrogenic marker gene expression was similar in both cell types (Figure S1G).

Comprehensive Gene Expression Analysis Reveals Step-by-Step Differentiation toward Chondrocytes
We next performed microarray analysis of sequential samples during the 2C differentiation. Hierarchical clustering
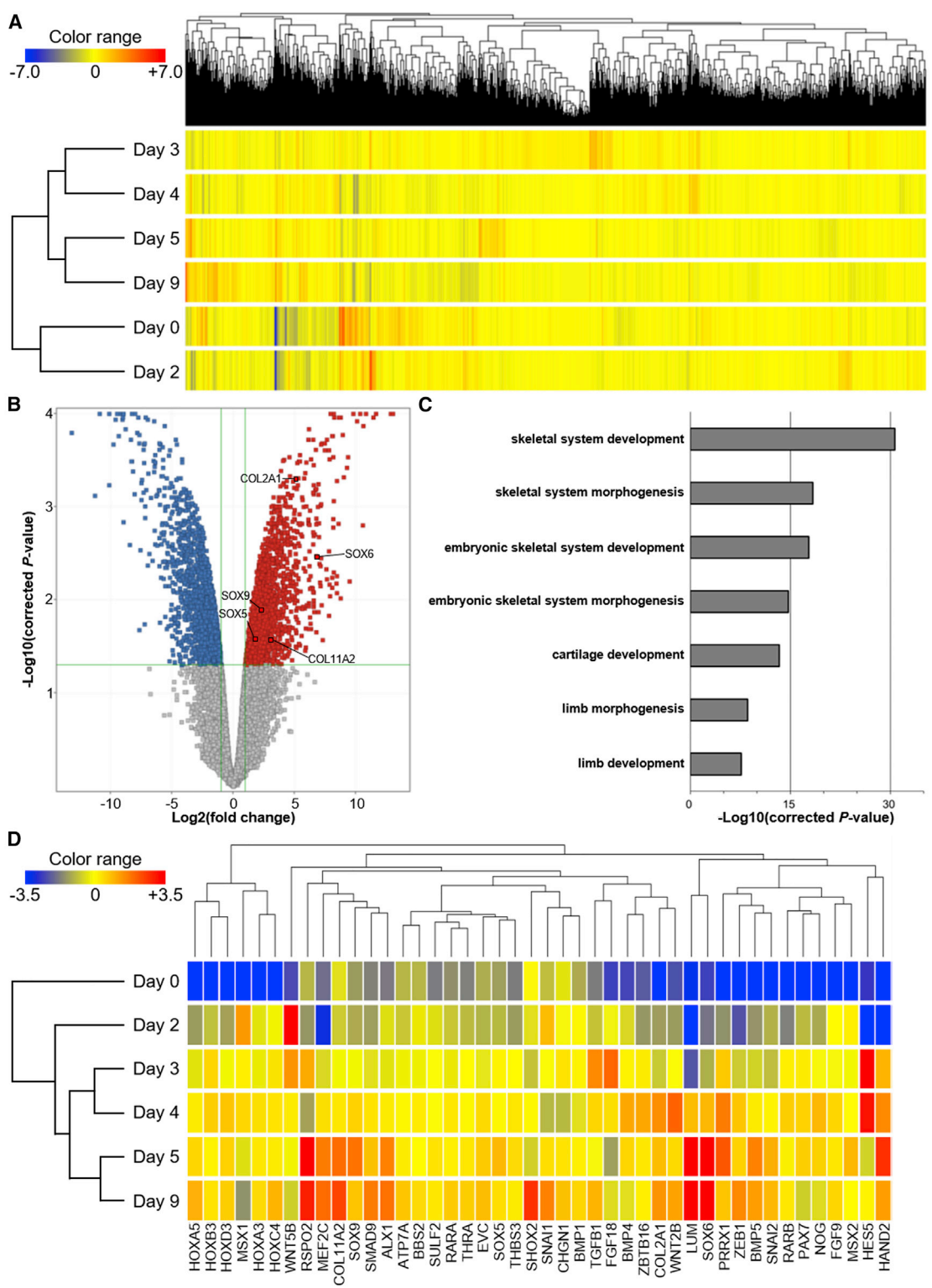
Figure 5. Microarray Analysis of Differentiation Induced by the 2C Protocol

(A) Hierarchical clustering analysis using all expressed genes in n = 3 sequential samples from three independent experiments during differentiation induced by the 2C protocol.

(legend continued on next page)

analysis for all expressed genes showed a distinct difference in expression profiles between samples before day 2 and after day 3 (Figure 5A). Volcano-plot analysis was performed to detect differentially expressed genes in the samples after differentiation compared with those on day 0, and this identified upregulated genes in each dataset (shown in sheets 1–5 of Table S1). For day-9 samples, 2,112 genes, including chondrogenic markers *SOX5*, *SOX6*, *SOX9*, *COL2A1*, and *COL11A2*, were found to be significantly upregulated (Figure 5B and sheet 5 of Table S1). Thereafter, gene ontology (GO) analysis using the upregulated genes of each day was performed (sheets 6–10 of Table S1). Skeletal-related terms, such as "skeletal system development" and "skeletal system morphogenesis," were highly enriched in all of the datasets, and "skeletal system development" was ranked top in the GO terms extracted from the day-9 dataset (Figure 5C and sheets 6–10 of Table S1). Terms relevant to cartilage formation, such as "cartilage development" and "cartilage morphogenesis," were also significantly enriched in each dataset, and among them, "cartilage development" was highly enriched with p = 4.50×10^{-14} in the upregulated genes of the day-9 samples (Figure 5C and sheets 6–10 of Table S1). Furthermore, hierarchical clustering analysis using the entities of "cartilage development" indicated that the expression profile of the day-9 samples was most similar to that of the day-5 samples, next in similarity to those of days 3 and 4, and most different from those of days 0 and 2 (Figure 5D). All of these findings were consistent with the step-by-step differentiation of hiPSCs toward chondrocytes under the 2C protocol.

Open Chromatin Analysis Shows that the 2C Protocol Induces Stepwise Chondrogenesis in Terms of Chromatin Accessibility

Assay for transposase-accessible chromatin using sequencing (ATAC-seq) was performed using hiPSC-derived cells during the 2C protocol to analyze sequential opening and closing of chromatin elements at each differentiation stage. The key features of each ATAC-seq dataset are summarized in sheet 1 of Table S2. About 35,000–47,000 raw peaks met the peak calling criteria for each dataset (sheet 2 of Table S2). A feature of peak distribution in the ATAC-seq datasets was striking enrichment around transcriptional start sites

(TSSs), as shown in sheet 3 of Table S2; approximately 28%–38% of all peaks lay within ±500 bp from a TSS (sheet 2 of Table S2), although this region represents only 0.001% of the genome (McLean et al., 2010). To focus on transcriptional regulation by distal enhancers during differentiation (Stadhouders et al., 2012), we extracted peaks more than 500 bp distant from a TSS for later analysis (sheets 2 and 4 of Table S2), as described previously (Ohba et al., 2015).

We performed Genomic Regions Enrichment of Annotations Tool (GREAT) GO analysis (McLean et al., 2010), using specific peaks in the samples after differentiation compared with those on day 0, to analyze stage-specific dynamics of chromatin accessibility (Figure 6A and sheets 6–23 of Table S2). Approximately 14,000–23,000 peaks in the samples after differentiation were distinct from those in day-0 samples (sheet 5 of Table S2), indicating that these distinct peaks represented characteristics of cells at each stage. The day-2-specific peak set compared with peaks in day-0 samples showed a strong association around genes related to GO Biological Process terms, such as "mesoderm morphogenesis" and "mesoderm formation" (sheet 6 of Table S2), indicating that day 2 was the mesoderm and mesendoderm stage, as shown by the gene expression analyses (Figures 2A and 5). Subsequently, "embryonic skeletal system morphogenesis" was highly enriched in the day-4- and day-5-specific peak sets (sheets 12 and 15 of Table S2). For the day-9-specific peaks, the highest ranked terms were "embryonic skeletal system development" and "embryonic skeletal system morphogenesis" (Figure 6A and sheet 21 of Table S2), while "regulation of chondrocyte differentiation" was enriched, with p = 1.47343×10^{-25} (sheet 21 of Table S2). For Mouse Phenotype and Human Phenotype annotations, terms relevant to skeletal formation were highly enriched in each peak set, and these terms monopolized the top four or five rankings of day-9-specific peaks (Figure 6A; sheets 7, 8, 10, 11, 13, 14, 16, 17, 19, 20, 22, and 23 of Table S2). These GREAT GO analysis findings indicated the step-by-step differentiation of hiPSCs toward chondrocytes via mesoderm and mesendoderm formation in the 2C protocol in terms of chromatin accessibility.

Next, we performed *de novo* motif analysis of day-9-specific peaks using MEME-ChIP (Bailey et al., 2009). A summary of the recovered motifs is shown in Figure S2A. It is

(B) Volcano-plot analysis to identify differentially expressed genes in the day-9 samples compared with those of day 0. Green lines indicate the threshold. Upregulated entities are shown as red dots and downregulated entities are indicated as blue dots; gray dots represent non-significantly differentially expressed genes.

(C) GO-term analysis of the upregulated genes in day-9 samples compared with those of day 0. The top seven enriched terms relevant to skeletal development and cartilage formation are shown.

(D) Hierarchical clustering analysis based on the gene set of "cartilage development" extracted from the upregulated genes in the day-9 dataset.

In (A) and (D), entities with increased expression are shown in red, and genes with decreased expression are shown in blue, as indicated by color-range bars. See also Table S1.
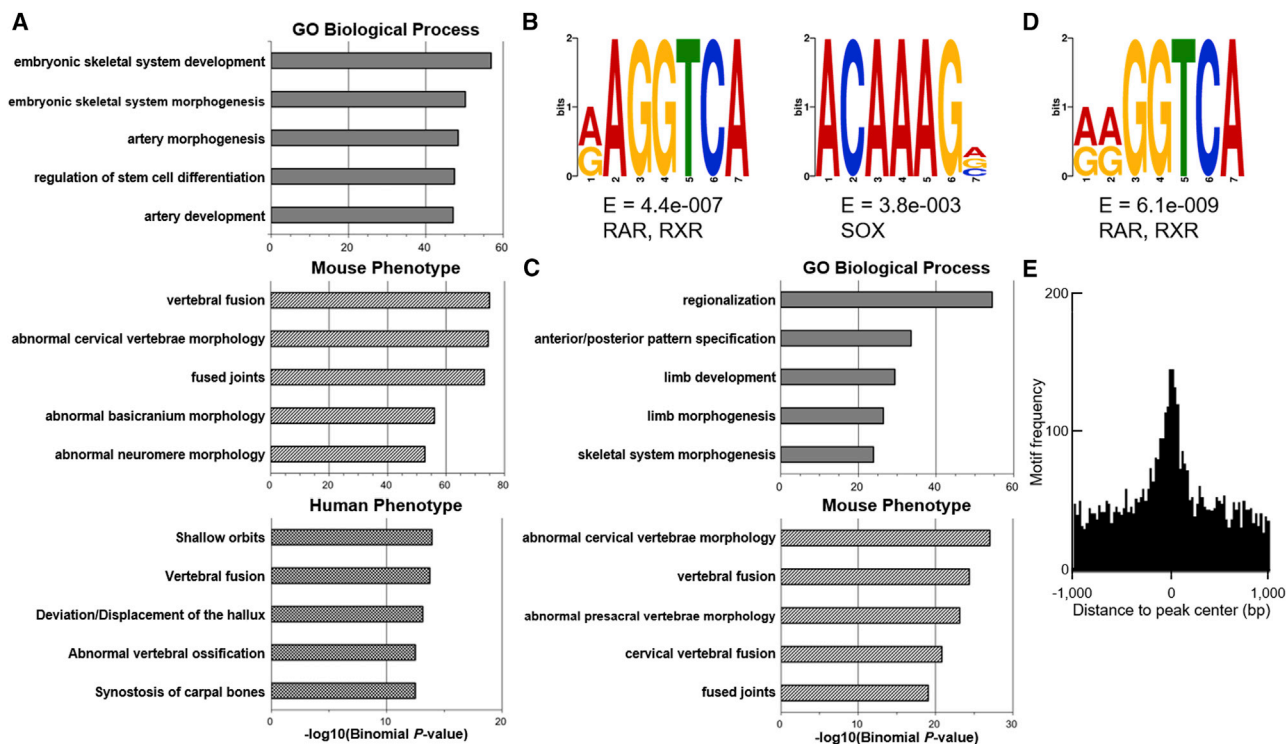
Figure 6. ATAC-Seq and RARα ChIP-Seq of hiPSC-Derived Cells on Day 9 of the 2C Protocol

(A) GREAT GO analysis of ATAC-seq peaks specific to day 9 compared with day 0. The top five enriched terms for GO Biological Process, Mouse Phenotype, and Human Phenotype are shown.

(B) SOX and RAR/RXR motifs recovered from ATAC-seq peaks of the day-9 MEME-ChIP analysis dataset. Motif logos display nucleotide frequencies (scaled relative to the information content) at each position.

(C) GREAT GO analysis of RARα ChIP-seq peaks in samples on day 9. The top five enriched terms for GO Biological Process and Mouse Phenotype are shown.

(D) A RAR/RXR motif recovered from RARα ChIP-seq peaks in the day-9 MEME-ChIP analysis dataset. Motif logos display nucleotide frequencies (scaled relative to the information content) at each position.

(E) Distribution of the RAR/RXR motif within a 1,000-bp window from the peak centers in RARα ChIP-seq peaks of the day-9 dataset. The numbers of existing motifs are shown on the y axis.

See also Figures S2 and S6; Tables S2, S3, and S4.

worth noting that the list of significantly enriched motifs included an RAR/RXR motif and an SOX motif (Figure 6B), indicating that enhancer elements specific to day 9 were potentially regulated by these factors.

Genome-wide Analysis Demonstrates RAR-DNA Association in Each Stage of the 2C Protocol

Chromatin immunoprecipitation sequencing (ChIP-seq) with an anti-human RARα antibody was performed using hiPSC-derived cells during the 2C differentiation to elucidate the roles of RARs in each stage of the 2C protocol. The key features of each dataset are summarized in sheet 1 of Table S2. Few peaks were enriched in the sample on day 0, and about 4,000–10,000 raw peaks met the peak calling criteria for each sample after day 2 (sheet 1 of Table S3). Peak distribution analysis revealed that, except for the

day-0 sample, only 8%–15% of the RARα-associated regions after day 2 occurred within 5 kb of TSSs (sheet 2 of Table S3), indicating that longer-range interactions were the predominant feature of the RARα regulatory program.

We performed GREAT GO analysis on the samples after differentiation (Figure 6C and sheets 3–20 of Table S3). The day-0 sample was excluded from the GREAT GO analysis because the number of peaks was very low. For GO Biological Process terms, the most highly ranked terms were "regionalization" and "anterior/posterior pattern specification" for all of the datasets (Figure 6C; sheets 3, 6, 9, 12, 15, and 18 of Table S3), which is consistent with the role of RA as a morphogen in embryogenesis (Bénazet and Zeller, 2009). Furthermore, highly significant recovery of terms related to limb development, skeletal system morphogenesis, and chondrocyte differentiation
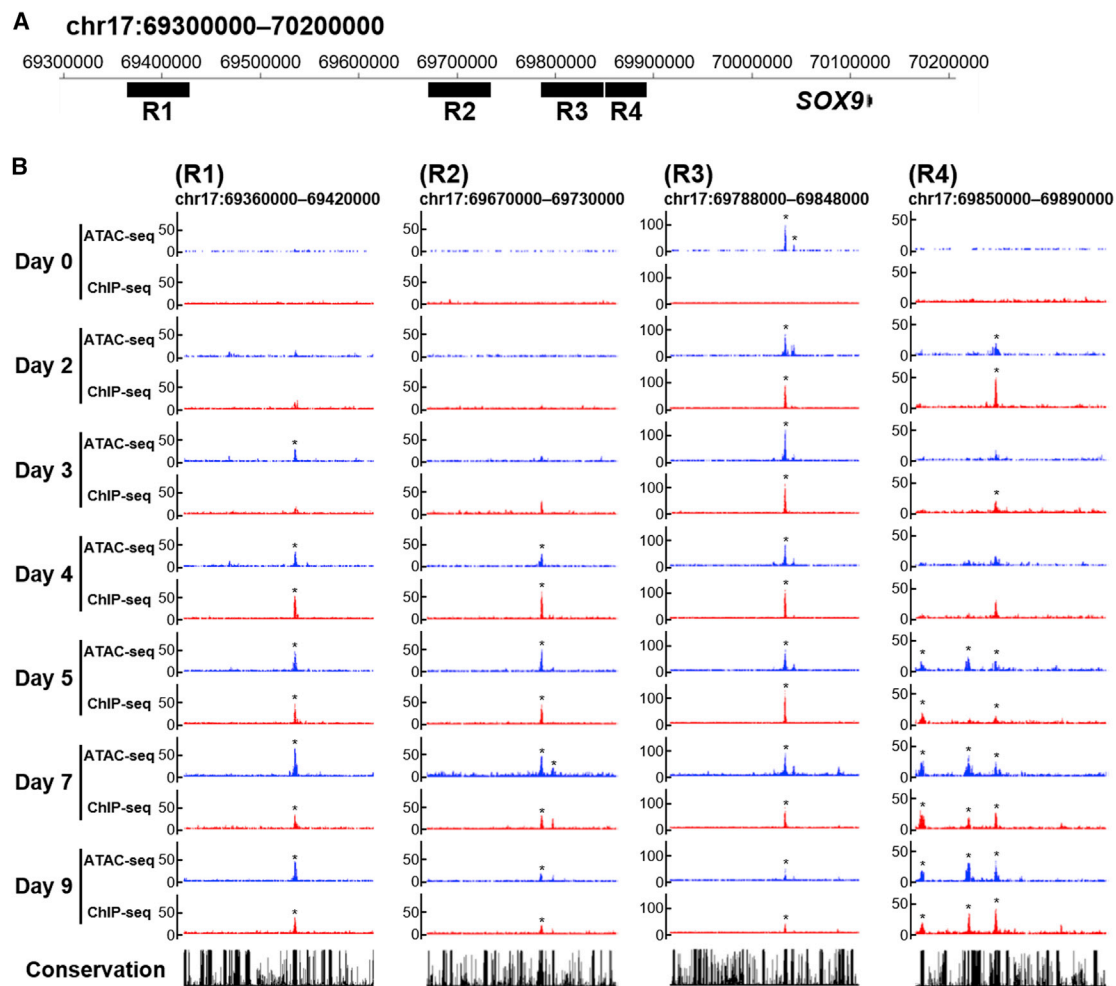
Figure 7. CisGenome Browser Views of Peaks for RARα ChIP-Seq and ATAC-Seq around *SOX9* during the 2C Differentiation
(A) Diagram of *SOX9* and regions including peaks (R1–R4) that were identified in the day-9 RARα ChIP-seq dataset and regarded as regulatory domains of *SOX9* by GREAT analysis.
(B) CisGenome browser screenshots showing R1–R4. Asterisks indicate peak regions that were putative regulatory domains of *SOX9* and common between the replicates.
See also Figures S3–S5 and S7.

was found in day-7 and day-9 peak sets (Figure 6C; sheets 15 and 18 of Table S3). For both Mouse Phenotype and Human Phenotype annotations, many terms relevant to skeletal formation were significantly enriched in each peak set, and terms regarding skeletal formation monopolized the top-five ranking of Mouse Phenotype in the day-9 peaks (Figure 6C; sheets 4, 5, 7, 8, 10, 11, 13, 14, 16, 17, 19, and 20 of Table S3).

De novo motif analysis of the day-9 peaks using MEME-ChIP identified an RAR/RXR motif (Figure 6D) among the significantly recovered motifs (Figure S2B). This motif was highly enriched at the predicted centers of the peaks (Figure 6E). These findings supported direct binding of RARα to enhancers as well as integrity of the ChIP-seq dataset.

RAR Binds to Enhancers in Mesendodermal, Mesodermal, and Chondrogenic Genes at Respective Differentiation Stages

We examined sequential changes of peak signals in ATAC-seq and RARα ChIP-seq around mesendodermal, mesodermal, and chondrogenic genes. Around *T* and *MIXL1*, regions with strong peak signals were seen on day 2 in both RARα ChIP-seq and ATAC-seq, and these signals became much weaker after day 3 (Figures S3A and S3B). Around *MEOX1*, there were peak regions on days 2–4, which were detected in RARα ChIP-seq and consistent with ATAC-seq (Figure S3C). Notably, several peak regions in both sequencing datasets overlapped around chondrogenic genes, such as *SOX9*, *SOX5*, and *SOX6*, after day 5

(Figures 7, S4, and S5). Collectively, these data demonstrate that RARα binds to enhancers around mesendodermal, mesodermal, and chondrogenic genes at respective differentiation stages of the 2C protocol.

β-Catenin ChIP-Seq Showed that Wnt/β-Catenin Signaling Regulated the Differentiation in Collaboration with RA Signaling

We hypothesized that collaborative effects of RA and Wnt/β-catenin signaling might be important for chondrocyte differentiation in the 2C protocol, as our optimization experiments with the two compounds showed that the efficiency of chondrocyte differentiation was lower when TTNPB was not present from the initiation of differentiation (Figure 1C). Therefore, β-catenin ChIP-seq was performed using hiPSC-derived cells on days 2 and 3 of the 2C differentiation to reveal the molecular roles of β-catenin in the 2C protocol. The key features of each dataset are summarized in sheets 1–3 of Table S4. Further analysis was not performed for the sample on day 3 because no significant peaks were enriched in the day-3 sample (sheet 2 of Table S4). A TCF (T cell factor) motif was top-ranked among the significantly recovered motifs in MEME-ChIP analysis of the day-2 peaks (Figure S6A), and this motif was highly enriched at the predicted centers of the peaks (Figure S6B), which supported the integrity of the β-catenin ChIP-seq dataset and suggested that Wnt/β-catenin signaling has a direct effect on enhancers.

Next, we examined peak signals in the putative enhancer regions of marker genes, including *T*, *MIXL1*, and *SOX9*, at each stage of differentiation. Some of the peaks identified in β-catenin ChIP-seq for the day-2 samples corresponded to those in the RARα ChIP-seq datasets on day 2 (Figures S6C, S6D, and S7A), which suggested that Wnt/β-catenin signaling directly regulated differentiation in the 2C protocol in coordination with RA signaling.

Essential Enhancer Regions Were Suggested by Epigenomic Analyses in Altered Protocols

To further reveal the importance of the coordination between Wnt/β-catenin and RA signaling in the 2C protocol, we performed β-catenin ChIP-seq, RARα ChIP-seq, and ATAC-seq with an altered 2C protocol whereby TTNPB was dosed from day 2 (TT(−) protocol, as shown in Figure S7B). We also executed RARα ChIP-seq with a protocol whereby CHIR99021 was not dosed (TT-only protocol, as shown in Figure S7B). We confirmed that the features of these datasets, which are summarized in sheets 1–3 of Table S4, were similar to those obtained with the standard 2C protocol. Peak analysis of these datasets showed that some of the open chromatin regions for ATAC-seq and the peak regions for ChIP-seq, identified in the standard protocol, were not found in the TT(−) or TT-only protocols

(Figures S6C, S6D, and S7A); this suggested that these regions might play essential roles in the differentiation process of the 2C protocol.

DISCUSSION

In the present study, we found that chondrocytes were robustly induced from hiPSCs by the simple combination of two small-molecule compounds, a GSK3 inhibitor and an RAR agonist, within 5–9 days. The differentiation induced by our protocol showed excellent efficiency and reproducibility among different hiPSC clones and mESCs. Particles prepared from hiPSC-derived differentiated cells formed hyaline cartilaginous tissues when transplanted into subcutaneous spaces and articular cartilage defects of mice. Real-time qRT-PCR, microarray analysis, and ATAC-seq showed that the time courses of gene expression and chromatin profiles were comparable with stepwise chondrogenesis through the mesendoderm and mesoderm stages. Furthermore, genome-wide analysis of RARα and β-catenin association with DNA demonstrated that RA and Wnt/β-catenin signaling collaboratively regulated the key marker genes at each differentiation stage.

Because RA is involved in the generation and differentiation of various tissues and organs, RA and retinoids have been used to induce differentiation of various cell types, including neural cells, photoreceptors, nephrogenic cells, and pancreatic cells (Araoka et al., 2014; D'Amour et al., 2006; Hu et al., 2009; Osakada et al., 2008; Tonge and Andrews, 2010). In some of these previous studies, RA was administered at intermediate and final stages, whereas in the 2C protocol we used TTNPB throughout differentiation. It is notable that the efficiency of chondrocyte differentiation deteriorated when TTNPB was not present from the beginning of the procedure. This finding may be compatible with a study describing that chondrogenic induction of mESC-derived embryoid bodies is promoted by treatment with RA in the early stage of differentiation (Kawaguchi et al., 2005). Optimal timing for RA or retinoid treatment in the induction protocols will differ by target cell type.

The effects of RA and retinoids on chondrogenesis or chondrocytes seem to largely depend on cell type and culture conditions. Some studies show that RA and retinoids promote hypertrophic differentiation and mineralization of cultured chondrocytes (Weston et al., 2003). They are also reported to have suppressive effects on collagen production or cartilage matrix synthesis in cultured chondrocytes or limb bud mesenchymal cells (Pacifici, 2018; Sekiya et al., 2001). Meanwhile, RA upregulates *SOX9* expression in a cartilage-derived cell line (Sekiya et al., 2000). To explain these discrepancies, it is assumed that primary chondrocytes contain heterogeneous

subpopulations while an established cell line consists of a homogeneous population of chondrocytes at a certain stage in which *SOX9* is enhanced by RA (Sekiya et al., 2001). Moreover, mouse genetic studies have contributed a series of findings about the indispensable functions of RA in chondrogenesis. In mice, knockout of retinaldehyde dehydrogenase-2 (Raldh2), an enzyme responsible for RA synthesis, results in lethality at mid-gestation accompanied by severely impaired development of various tissues and organs (Niederreither et al., 1999). Limb buds do not form, and subsequent chondrogenesis and endochondral ossification does not occur in *Raldh2*-deficient embryos (Niederreither et al., 1999). Notably, RA supplementation during embryonic days 7.5–10.5 markedly rescues chondrogenesis and endochondral ossification of *Raldh2*-deficient embryos (Niederreither et al., 2002). In addition, *in vivo* experiments using knockout mice for RARs support the roles of these receptors in chondrocyte differentiation. Although single-knockout mice for each RAR do not show abnormal development, a double knockout for RARα and RARγ has severely impaired skeletal growth (Lohnes et al., 1994). Taken together, these findings show that RA is essential for the entire process of chondrocyte differentiation. Considering the present data of time-course gene expression and open chromatin profiles, serial induction from PSCs toward chondrocytes by the 2C protocol probably may mimic these physiological functions of RA throughout chondrogenesis.

The binding of RAR to enhancers in mesendodermal, mesodermal, and chondrogenic genes at each stage during the 2C differentiation, displayed by the ChIP-seq datasets, indicates the molecular roles of RA throughout the chondrogenic process, which is consistent with the previous studies described above (Lohnes et al., 1994; Niederreither et al., 1999, 2002). As for mesodermal genes, it is reported that *MEOX1* is induced by RA (Dixon et al., 2017), which is compatible with the present study. Meanwhile, *SOX9* enhancers for various organs have been identified, including testis, gonad (Sekido and Lovell-Badge, 2008), midbrain, telencephalon, hindbrain, spinal cord, node, notochord, gut, bronchial epithelium, pancreas, cranial neural crest, inner ear (Bagheri-Fam et al., 2006), and cartilage or chondrocytes (Mochizuki et al., 2018; Yao et al., 2015). Although binding sites for RA or Wnt/β-catenin signaling shown in the present study seem to not correspond to these reported enhancers, the differences of chromatin accessibility and RAR and β-catenin association with DNA between the standard 2C protocol and the altered 2C protocols may suggest enhancer regions that are essential for chondrocyte differentiation via the mesendoderm and mesoderm stages. Furthermore, the finding that the putative genes regulated by RAR at each differentiation stage included key marker genes for each developmental stage implies that RA

signaling is involved in fundamental regulation of chondrogenesis. The mechanisms for this may be attributed to the changes of chromatin modification or structure in each differentiation stage, and future thorough studies are expected to elucidate the intriguing regulatory function of RAR during chondrogenesis.

Similarly, CHIR99021 has been employed in various protocols for PSC differentiation to neural cells, hemogenic endothelial progenitors, nephrogenic intermediate mesodermal cells, and osteoblasts (Araoka et al., 2014; Kanke et al., 2014; Kirkeby et al., 2012; Kitajima et al., 2016; Xi et al., 2012). Characteristics of the induced neural cells greatly differ by doses and periods of CHIR99021 treatment (Xi et al., 2012). Our optimization experiments showed that higher doses of CHIR99021 and shorter treatment periods were required for efficient chondrocyte differentiation, compared with conditions previously described for neural cell induction (Kirkeby et al., 2012; Xi et al., 2012). Furthermore, considering that different doses, timings, and treatment periods in the protocols using CHIR99021 and TTNPB can lead to induction of different types of cells, such as chondrocytes in our study and nephrogenic intermediate mesodermal cells previously (Araoka et al., 2014), these two compounds may be useful for inducing various cell types when administered under different conditions. The time-course analysis by real-time qRT-PCR showed that expression of marker genes was rapidly altered at each differentiation stage in the 2C protocol. Microarray analysis and ATAC-seq showed that hiPSCs differentiated in a stepwise manner toward chondrocytes via mesendoderm and mesoderm stages. These findings indicate that the differentiation of hiPSCs induced by the 2C protocol is consistent with step-by-step chondrogenesis during embryogenesis (Craft et al., 2015; Oldershaw et al., 2010; Yamashita et al., 2015). Therefore, the present method should be useful as an *in vitro* experimental model of differentiation from PSCs toward chondrocytes. Meanwhile, chondrocytes are known to differentiate from multiple lineages, including paraxial and lateral plate mesoderms, and multistage chondrocyte induction models tracing a specific lineage of differentiation have been proposed in some studies (Craft et al., 2015; Loh et al., 2016; Umeda et al., 2012; Winslow et al., 2007; Xi et al., 2017; Zhao et al., 2014). However, the 2C protocol is the simple combination of two compounds, and we consider that this method will not trace specific lineages during the differentiation, as marker genes for both paraxial and lateral plate mesoderms were upregulated. Instead, Wnt and RA signaling might play essential regulatory roles that are common among the multiple lineages of chondrogenesis. Further mechanistic studies of the two signaling pathways or detailed analyses of the interaction between these pathways may contribute to explication of the molecular mechanisms underlying the chondrogenesis and differentiation.

The 2C protocol produced more homogeneous differentiation when compared with previously reported methods using cytokines (Oldershaw et al., 2010; Yamashita et al., 2015). This is probably because small-molecule compounds regulate cells directly instead of through complicated signal transduction processes triggered by cytokine-receptor interactions. The cells differentiated by the 2C protocol had the potential to form hyaline cartilaginous tissues in articular cartilage defects in mouse knees, although partial replacement with host mouse chondrocytes and remodeling of the articular surface appeared to occur because of the higher turnover of chondrocytes in small animals, as described in similar previous experiments (Toh et al., 2010; Yamashita et al., 2015). Furthermore, the hiPSC-derived grafts in subcutaneous spaces formed hyaline cartilaginous tissues surrounded by layers expressing Lubricin. This two-layer structure may be similar to that described in subcutaneous transplantation of hiPSC-derived particles in another study (Yamashita et al., 2015), although immunofluorescence of Lubricin was not examined in this study. The grafts may undergo hypertrophy or ossification if transplanted to more vascularized tissues, e.g., the renal capsule described in another study (Colnot et al., 2004). However, the ability to form hyaline cartilaginous tissues *in vivo* and to repair articular cartilage defects, both shown in the present study, are beneficial for clinical application in various areas. Therefore, the 2C protocol is a promising method for providing an unlimited and safe source of cells for cartilage regenerative medicine at low cost. Production of cartilage tissues of various sizes and types, by combining the present differentiation method with appropriate tissue engineering techniques and additional factors, is an important goal of future research.

EXPERIMENTAL PROCEDURES

Detailed experimental procedures are provided in Supplemental Information.

Ethics Statement

We performed all mouse experiments according to a protocol approved by the Animal Care and Use Committee of The University of Tokyo. We obtained human bone and adipose tissue from individuals undergoing knee arthroplasty with written informed consent as approved by the Ethics Committee of The University of Tokyo.

ACCESSION NUMBERS

The raw microarray data are deposited in the Gene Expression Omnibus under accession number GEO: GSE96036. ATAC-seq and ChIP-seq data are deposited under accession numbers GEO: GSE109172 and GSE132532.

REFERENCES

Araoka, T., Mae, S., Kurose, Y., Uesugi, M., Ohta, A., Yamanaka, S., and Osafune, K. (2014). Efficient and rapid induction of human iPSCs/ESCs into nephrogenic intermediate mesoderm using small molecule-based differentiation methods. PLoS One *9*, e84881.

Bagheri-Fam, S., Barrionuevo, F., Dohrmann, U., Günther, T., Schüle, R., Kemler, R., Mallo, M., Kanzler, B., and Scherer, G. (2006). Long-range upstream and downstream enhancers control distinct subsets of the complex spatiotemporal Sox9 expression pattern. Dev. Biol. *291*, 382–397.

Bailey, T.L., Boden, M., Buske, F.A., Frith, M., Grant, C.E., Clementi, L., Ren, J., Li, W.W., and Noble, W.S. (2009). MEME SUITE: tools for motif discovery and searching. Nucleic Acids Res. *37*, W202–W208.

Bakre, M.M., Hoi, A., Mong, J.C., Koh, Y.Y., Wong, K.Y., and Stanton, L.W. (2007). Generation of multipotential mesendodermal progenitors from mouse embryonic stem cells via sustained Wnt pathway activation. J. Biol. Chem. *282*, 31703–31712.

Bridgewater, L.C., Lefebvre, V., and de Crombrugghe, B. (1998). Chondrocyte-specific enhancer elements in the Col11a2 gene

resemble the Col2a1 tissue-specific enhancer. J. Biol. Chem. *273*, 14998–15006.

Bénazet, J.D., and Zeller, R. (2009). Vertebrate limb development: moving from classical morphogen gradients to an integrated 4-dimensional patterning system. Cold Spring Harb. Perspect. Biol. *1*, a001339.

Cao, N., Huang, Y., Zheng, J., Spencer, C.I., Zhang, Y., Fu, J.D., Nie, B., Xie, M., Zhang, M., Wang, H., et al. (2016). Conversion of human fibroblasts into functional cardiomyocytes by small molecules. Science *352*, 1216–1220.

Colnot, C., Lu, C., Hu, D., and Helms, J.A. (2004). Distinguishing the contributions of the perichondrium, cartilage, and vascular endothelium to skeletal development. Dev. Biol. *269*, 55–69.

Craft, A.M., Rockel, J.S., Nartiss, Y., Kandel, R.A., Alman, B.A., and Keller, G.M. (2015). Generation of articular chondrocytes from human pluripotent stem cells. Nat. Biotechnol. *33*, 638–645.

D'Amour, K.A., Bang, A.G., Eliazer, S., Kelly, O.G., Agulnick, A.D., Smart, N.G., Moorman, M.A., Kroon, E., Carpenter, M.K., and Baetge, E.E. (2006). Production of pancreatic hormone-expressing endocrine cells from human embryonic stem cells. Nat. Biotechnol. *24*, 1392–1401.

Dixon, K., Chen, J., and Li, Q. (2017). Gene expression profiling discerns molecular pathways elicited by ligand signaling to enhance the specification of embryonic stem cells into skeletal muscle lineage. Cell Biosci. *7*, 23.

Hu, B.Y., Du, Z.W., and Zhang, S.C. (2009). Differentiation of human oligodendrocytes from pluripotent stem cells. Nat. Protoc. *4*, 1614–1622.

Kanke, K., Masaki, H., Saito, T., Komiyama, Y., Hojo, H., Nakauchi, H., Lichtler, A.C., Takato, T., Chung, U.I., and Ohba, S. (2014). Stepwise differentiation of pluripotent stem cells into osteoblasts using four small molecules under serum-free and feeder-free conditions. Stem Cell Reports *2*, 751–760.

Kawaguchi, J., Mee, P.J., and Smith, A.G. (2005). Osteogenic and chondrogenic differentiation of embryonic stem cells in response to specific growth factors. Bone *36*, 758–769.

Kirkeby, A., Grealish, S., Wolf, D.A., Nelander, J., Wood, J., Lundblad, M., Lindvall, O., and Parmar, M. (2012). Generation of regionally specified neural progenitors and functional neurons from human embryonic stem cells under defined conditions. Cell Rep. *1*, 703–714.

Kitajima, K., Nakajima, M., Kanokoda, M., Kyba, M., Dandapat, A., Tolar, J., Saito, M.K., Toyoda, M., Umezawa, A., and Hara, T. (2016). GSK3β inhibition activates the CDX/HOX pathway and promotes hemogenic endothelial progenitor differentiation from human pluripotent stem cells. Exp. Hematol. *44*, 68–74.e1-10.

Lefebvre, V., Huang, W., Harley, V.R., Goodfellow, P.N., and de Crombrugghe, B. (1997). SOX9 is a potent activator of the chondrocyte-specific enhancer of the pro alpha1(II) collagen gene. Mol. Cell. Biol. *17*, 2336–2346.

Loh, K.M., Chen, A., Koh, P.W., Deng, T.Z., Sinha, R., Tsai, J.M., Barkal, A.A., Shen, K.Y., Jain, R., Morganti, R.M., et al. (2016). Mapping the pairwise choices leading from pluripotency to human bone, heart, and other mesoderm cell types. Cell *166*, 451–467.

Lohnes, D., Mark, M., Mendelsohn, C., Dollé, P., Dierich, A., Gorry, P., Gansmuller, A., and Chambon, P. (1994). Function of the retinoic acid receptors (RARs) during development (I). Craniofacial and skeletal abnormalities in RAR double mutants. Development *120*, 2723–2748.

McLean, C.Y., Bristor, D., Hiller, M., Clarke, S.L., Schaar, B.T., Lowe, C.B., Wenger, A.M., and Bejerano, G. (2010). GREAT improves functional interpretation of cis-regulatory regions. Nat. Biotechnol. *28*, 495–501.

Mochizuki, Y., Chiba, T., Kataoka, K., Yamashita, S., Sato, T., Kato, T., Takahashi, K., Miyamoto, T., Kitazawa, M., Hatta, T., et al. (2018). Combinatorial CRISPR/Cas9 approach to elucidate a far-upstream enhancer complex for tissue-specific Sox9 expression. Dev. Cell *46*, 794–806.e6.

Niederreither, K., Subbarayan, V., Dollé, P., and Chambon, P. (1999). Embryonic retinoic acid synthesis is essential for early mouse post-implantation development. Nat. Genet. *21*, 444–448.

Niederreither, K., Vermot, J., Schuhbaur, B., Chambon, P., and Dollé, P. (2002). Embryonic retinoic acid synthesis is required for forelimb growth and anteroposterior patterning in the mouse. Development *129*, 3563–3574.

Ohba, S., He, X., Hojo, H., and McMahon, A.P. (2015). Distinct transcriptional programs underlie Sox9 regulation of the mammalian chondrocyte. Cell Rep. *12*, 229–243.

Oldershaw, R.A., Baxter, M.A., Lowe, E.T., Bates, N., Grady, L.M., Soncin, F., Brison, D.R., Hardingham, T.E., and Kimber, S.J. (2010). Directed differentiation of human embryonic stem cells toward chondrocytes. Nat. Biotechnol. *28*, 1187–1194.

Osakada, F., Ikeda, H., Mandai, M., Wataya, T., Watanabe, K., Yoshimura, N., Akaike, A., Sasai, Y., and Takahashi, M. (2008). Toward the generation of rod and cone photoreceptors from mouse, monkey and human embryonic stem cells. Nat. Biotechnol. *26*, 215–224.

Pacifici, M. (2018). Retinoid roles and action in skeletal development and growth provide the rationale for an ongoing heterotopic ossification prevention trial. Bone *109*, 267–275.

Saito, T., Yano, F., Mori, D., Kawata, M., Hoshi, K., Takato, T., Masaki, H., Otsu, M., Eto, K., Nakauchi, H., et al. (2015). Hyaline cartilage formation and tumorigenesis of implanted tissues derived from human induced pluripotent stem cells. Biomed. Res. *36*, 179–186.

Sekido, R., and Lovell-Badge, R. (2008). Sex determination involves synergistic action of SRY and SF1 on a specific Sox9 enhancer. Nature *453*, 930–934.

Sekiya, I., Tsuji, K., Koopman, P., Watanabe, H., Yamada, Y., Shinomiya, K., Nifuji, A., and Noda, M. (2000). SOX9 enhances aggrecan gene promoter/enhancer activity and is up-regulated by retinoic acid in a cartilage-derived cell line, TC6. J. Biol. Chem. *275*, 10738–10744.

Sekiya, I., Koopman, P., Tsuji, K., Mertin, S., Harley, V., Yamada, Y., Shinomiya, K., Niguji, A., and Noda, M. (2001). Transcriptional suppression of Sox9 expression in chondrocytes by retinoic acid. J. Cell. Biochem. *Suppl 36*, 71–78.

Stadhouders, R., van den Heuvel, A., Kolovos, P., Jorna, R., Leslie, K., Grosveld, F., and Soler, E. (2012). Transcription regulation by distal enhancers: who's in the loop? Transcription *3*, 181–186.

Toh, W.S., Lee, E.H., Guo, X.M., Chan, J.K., Yeow, C.H., Choo, A.B., and Cao, T. (2010). Cartilage repair using hyaluronan hydrogel-encapsulated human embryonic stem cell-derived chondrogenic cells. Biomaterials *31*, 6968–6980.

Tonge, P.D., and Andrews, P.W. (2010). Retinoic acid directs neuronal differentiation of human pluripotent stem cell lines in a non-cell-autonomous manner. Differentiation *80*, 20–30.

Umeda, K., Zhao, J., Simmons, P., Stanley, E., Elefanty, A., and Nakayama, N. (2012). Human chondrogenic paraxial mesoderm, directed specification and prospective isolation from pluripotent stem cells. Sci. Rep. *2*, 455.

Weston, A.D., Hoffman, L.M., and Underhill, T.M. (2003). Revisiting the role of retinoid signaling in skeletal development. Birth Defects Res. C Embryo Today *69*, 156–173.

Winslow, B.B., Takimoto-Kimura, R., and Burke, A.C. (2007). Global patterning of the vertebrate mesoderm. Dev. Dyn. *236*, 2371–2381.

Xi, J., Liu, Y., Liu, H., Chen, H., Emborg, M.E., and Zhang, S.C. (2012). Specification of midbrain dopamine neurons from primate pluripotent stem cells. Stem Cells *30*, 1655–1663.

Xi, H., Fujiwara, W., Gonzalez, K., Jan, M., Liebscher, S., Van Handel, B., Schenke-Layland, K., and Pyle, A.D. (2017). In vivo human somitogenesis guides somite development from hPSCs. Cell Rep. *18*, 1573–1585.

Yamashita, A., Morioka, M., Yahara, Y., Okada, M., Kobayashi, T., Kuriyama, S., Matsuda, S., and Tsumaki, N. (2015). Generation of scaffoldless hyaline cartilaginous tissue from human iPSCs. Stem Cell Reports *4*, 404–418.

Yao, B., Wang, Q., Liu, C.F., Bhattaram, P., Li, W., Mead, T.J., Crish, J.F., and Lefebvre, V. (2015). The SOX9 upstream region prone to chromosomal aberrations causing campomelic dysplasia contains multiple cartilage enhancers. Nucleic Acids Res. *43*, 5394–5408.

Zhao, Q., Eberspaecher, H., Lefebvre, V., and De Crombrugghe, B. (1997). Parallel expression of Sox9 and Col2a1 in cells undergoing chondrogenesis. Dev. Dyn. *209*, 377–386.

Zhao, J., Li, S., Trilok, S., Tanaka, M., Jokubaitis-Jameson, V., Wang, B., Niwa, H., and Nakayama, N. (2014). Small molecule-directed specification of sclerotome-like chondroprogenitors and induction of a somitic chondrogenesis program from embryonic stem cells. Development *141*, 3848–3858.